Atmospheric Environment 268 (2022) 118770

Contents lists available at ScienceDirect

Atmospheric Environment

journal homepage: www.elsevier.com/locate/atmosenv

Aerosol characterization in an oceanic context around Reunion Island (AEROMARINE field campaign)

Faustine Mascaut [a], Olivier Pujol [a], Bert Verreyken [b,c,d], Raphaël Peroni [a], Jean Marc Metzger [e], Luc Blarel [a], Thierry Podvin [a], Philippe Goloub [a], Karine Sellegri [f], Troy Thornberry [g,h], Valentin Duflot [b], Pierre Tulet [i], Jérôme Brioude [b,*]

[a] Université de Lille, Département de Physique, Laboratoire d'Optique Atmosphérique (LOA), 59655, Villeneuve d'Ascq, France
[b] Laboratoire de l'Atmosphère et des Cyclones (LACy), UMR 8105, Météo France/CNRS/Université de La Réunion, St Denis de La Réunion, France
[c] Royal Belgian Institute for Space Aeronomy, 1180, Brussels, Belgium
[d] Department of Chemistry, Ghent University, 9000, Ghent, Belgium
[e] Observatoire des Sciences de l'Univers de La Réunion, UMS3365, 97744, St Denis, France
[f] Laboratoire de Météorologie Physique, Observatoire de Physique du Globe de Clermont-Ferrand, Université Blaise Pascal – CNRS, 63177, Aubière, France
[g] NOAA Chemical Sciences Laboratory (CSL), Boulder, USA
[h] CIRES, University of Colorado Boulder, Boulder, USA
[i] Laboratoire d'Aérologie, Université de Toulouse, UT3, CNRS, IRD, 31400, Toulouse, France

HIGHLIGHTS

- Optical properties, vertical distribution and transport pathways, from the marine boundary layer to the free troposphere, of marine aerosols in a pristine environment are examined.
- Aerosol size does not exceed the accumulation mode.
- A sketch is proposed as a characterization of marine aerosols distribution. Oceanic and insular influences in the aerosol content are separated.
- It is argued that the AERONET station at St Denis (Reunion Island) is well representative of marine conditions.
- With data from a microwave radiometer, water vapour-aerosol-cloud models in a pristine ocean can be feeded.

GRAPHICAL ABSTRACT

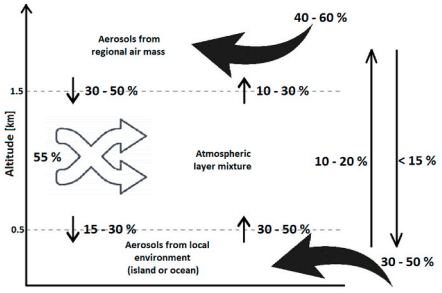

ARTICLE INFO

Keywords:
Sea salt aerosols
Pristine conditions
Southern indian Ocean
AEROMARINE field Campaign

ABSTRACT

This article presents the results of the AEROMARINE field campaign which took place between February and April 2019 off the coast of Reunion Island in the South West Indian Ocean basin. The Southern Indian Ocean is of major interest for the study of marine aerosols, their distribution and variability. Six instrumented light plane flights and a ground-based microwave radiometer were used during the field campaign. These measurements were compared with the long-term measurements of the AERONET sun-photometer (based in St Denis, Reunion Island) and various instruments of the high altitude Maïdo Observatory (2.2 km above sea level, Reunion Island). These results were also analyzed using different model outputs: (i) the AROME mesoscale weather forecast model

* Corresponding author.
E-mail address: jerome.brioude@univ-reunion.fr (J. Brioude).

https://doi.org/10.1016/j.atmosenv.2021.118770
Received 29 July 2021; Accepted 26 September 2021
Available online 3 October 2021

to work on the thermodynamics of the boundary layer, (ii) the FLEXPART-AROME Lagrangian particle dispersion model to assess the geographical and vertical origin of air masses, and (iii) the chemical transport model CAMS (Copernicus Atmosphere Monitoring Service) to work on the aerosol chemical composition of air masses. This allowed to highlight two points: (1) the atmospheric layer above 1.5 km is mainly composed of aerosols from the regional background; (2) the local environment (ocean or island) has little impact on the measured concentrations. Marine aerosols emitted locally are mostly measured below 0.5 km. The daytime marine aerosol distributions in the free troposphere measured by the aircraft were compared to the night-time aerosol distributions measured at the high altitude Maïdo Observatory when the Observatory is located in the free troposphere. The results indicate that this high altitude site of measurements is representative of the marine aerosol concentrations in the free troposphere. We also found that the CAMS reanalyses overestimated the aerosol optical depth in this region. Finally, our study strongly suggests that the AERONET station in St Denis (Reunion Island) can be considered as a representative marine station under the Tropics.

Acronyms

AERONET	AErosol RObotic NETwork
AODs	Aerosol Optical Depths
CAMS	Copernicus Atmosphere Monitoring Service.
CPC	Condensable Particle Counter
MAP-IO	Marion Dufresne Atmospheric Program - Indian Ocean
MBL	Marine Boundary Layer
MWRP	MicroWave Radiometer Profiler
OM	Organic Matter
PLASMA	Photomètre LégerAéroporté pour la Surveillance des Masses d'Air
POPS	Portable Optical Particle Counter
SSA	Sea Salt Aerosols
SST	Sea Surface Temperature
TAF	Terres Australes Françaises

1. Introduction

Because of their direct and indirect radiative forcings, atmospheric aerosols have a major impact on the climate. These forcings are still poorly understood and lead to uncertainties that have persisted in models since the 1990s (Myhre et al., 2013). One of the largest uncertainties of the aerosol-cloud system is the background concentration of natural aerosols, especially over clean marine regions (Andreae and Rosenfeld, 2008). Oceans cover about 70% of the Earth's surface and are an important reservoir of marine aerosols (mainly sea salt and organic aerosols). Sea Salt Aerosols (SSA) are one of the largest contributors to global aerosol loading and, therefore, they play an important role in global climate. Also, they were proposed to be a major component of primary marine aerosol mass over the regions where wind speeds are high and/or other aerosol sources are weak (Gantt and Meskhidze, 2013; O'Dowd and de Leeuw, 2007). Luo et al. (2014) showed that the *AOD* at 532 nm of SSA in the Marine Boundary Layer (MBL) is governed by different physical factors: the surface wind speed, the Sea Surface Temperature (SST), the MBL height, the lower troposphere stability, and the relative humidity (impact on size and optical properties of sea salt particles). However, there is a notable lack of data, in particular over the oceans and in the Southern Hemisphere, describing the characteristics of aerosols such as optical properties, size distribution, temporal and spatial variabilities (Ramachandran, 2004). Pant et al. (2009) carried out measurements of the total number concentration and the size distribution of aerosols over the Indian Ocean in 2004. They observed that the aerosol concentration-wind speed correlation coefficient depends on the latitude and has a maximum value where winds are the strongest.

The southwestern Indian Ocean has been identified as a region with frequent pristine conditions (where land and human activities have little impact) that can reasonably be considered to be close to the preindustrial conditions. Few data have been collected in this region (Pant et al., 2009). However, it is a crucial reference point to quantify the background concentration of natural aerosols and the contribution of natural emissions to the changing climate. In pristine regions, SSA are dominant and concentrations are relatively low (*e.g.* Mallet et al., 2018).

Reunion Island in the southwestern Indian Ocean can be considered as a background aerosol pristine environment under trade wind conditions (Koren et al., 2014), mostly during the wet season from December to April. For details about wind circulation in the Southern Indian Ocean, including Reunion Island, see the statistical study by Mallet et al. (2018) and refs therein. Reunion Island is also a unique site in the Southern Hemisphere for making aerosol observations. Indeed, being in an oceanic environment and far from continents, the Island is in a strategic location for carrying out measurements in a clean region, and also for the validation of spatial measurements. In addition, the Maïdo Observatory (located at 2.2 km above sea level (a.s.l)[1]) allows: (i) to take measurements directly in the free troposphere at night (Guilpart et al., 2017; Foucart et al., 2018) and (ii) to perform long-term *in-situ* observations including detailed profiles of wind, temperature and water, as well as concentration, size and chemical composition of aerosols collected by ground instruments (Baray et al., 2013).

The AEROMARINE project, which took place between February and April 2019, aimed at collecting data on marine aerosol emissions, their optical properties, their transport and distribution off the coast of Reunion Island. For this, ground-based instruments and instruments on board ultra light plane were used to measure concentration, size distribution and optical thickness of marine aerosols over the Indian Ocean, on the western side of Reunion Island. In addition, in order to characterize the thermodynamics of the MBL and the exchanges between the MBL and the free troposphere, a MicroWave Radiometer Profiler (MWRP) was set up in St Denis (in the north of the Island). Aerosol data have been complemented by the measurements of the AErosol RObotic NETwork (AERONET) sun-photometer (St Denis) and the various instruments of the Maïdo Observatory. Models, such as FLEXPART-MesoNH or AROME as well as Copernicus Atmosphere Monitoring Service (CAMS) reanalyses, allowed to compare and/or support *in-situ* measurements. The instruments (on board and on the ground) and the models used are briefly presented in the following section.

The overall objectives of the AEROMARINE project include:

1) To characterize marine aerosol optical properties and their vertical distribution. The instruments on board the light plane helped characterize the marine aerosol optical properties, number concentration, and size distribution within the MBL and the free troposphere. Those results were compared with aerosol measurements at the Maïdo Observatory. Furthermore, *AOD*-measurements were compared with those of the AERONET station at St Denis.
2) To examine the transport pathways of marine aerosols from the boundary layer to the free troposphere. Hence, it is important to estimate accurately the vertical distribution of the marine aerosols.

[1] In this paper, altitudes are given above sea level (a.s.l).

Indeed, the MBL dynamics affect marine emission mechanisms, vertical dilution, while shallow convection is important for exchange and mixing of aerosols with the free troposphere.

The aim of this paper is to present the results obtained (Section 3) during AEROMARINE that answer the above objectives. Section 4 is the conclusion of this work.

2. Instruments and models used

2.1. On-board instruments

2.1.1. PLASMA

Photomètre Léger Aéroporté pour la Surveillance des Masses d'Air (PLASMA) is a sun-tracking photometer developed by LOA and SNO PHOTONS (Karol et al., 2013). Compact (23 cm) and light (3 kg), it can be put on different mobile platforms (Popovici et al., 2018). Sun tracking is performed by means of elevation ($0 - 88°$) and azimuth ($0 - 360°$) rotations. Aerosol Optical Depths (*AODs*) at various wavelengths[2] (λ) are derived from extinction measurements of the solar radiation by molecular and aerosol scattering and absorption processes. The instrument provides *AODs* over a wide spectral range ($\lambda = 0.34 - 2.25\ \mu$m) with an accuracy ΔAOD ranging from 0.005 to 0.01 according to λ. Aerosol size distribution is retrieved from the *AOD* spectral dependence (Karol et al., 2013). The Angström exponent α is determined from the law of Angström: $AOD_1/\mathrm{AOD}_2 = (\lambda_1/\lambda_2)^{-\alpha}$ where AOD_i is the aerosol optical depth at the wavelength λ_i (AngstrÖm, 1961). This exponent describes how the *AOD* varies with λ and so provides information on the size distribution of the aerosols (Kusmierczyk-Michulec et al., 2002).

2.1.2. Particle counters

The Portable Optical Particle Counter (POPS) is a 900 g *in situ* instrument designed by US laboratories NOAA and CIRES that provides aerosol number size distribution (in the size range 132 nm – 3 μm) using single-particle light scattering (Gao et al., 2016). POPS is a prototype made by a 3D printer to reduce weight. It flew on board a light plane during the AEROMARINE campaign within the MBL and the free troposphere.

Two Condensable Particle Counters (CPCs) (accuracy: ± 20%) are used simultaneously to measure the total concentration of particles larger than 2 nm (CPC-MAGIC200) and particles larger than 10 nm (CPC TSI model 3007). The difference of concentration between the two CPCs gives the particle concentration in the size range 2 – 10 nm, which is indicative of the recent formation of nanometric particles, i.e. nucleation. The combination of two CPCs to investigate nucleation was proven to be adequate in past airborne studies (Crumeyrolle et al., 2010). Additionally, in synergy with the POPS, the CPC TSI 3007 concentration enables to measure the aerosol concentration in the 10–150 nm size range, which is indicative of grown nucleated particles, and fine marine primary aerosols (size range 50 – 100 nm) that dominate the primary marine aerosol size distribution (Schwier et al., 2017).

2.2. Ground-based instruments

2.2.1. AERONET stations

The AERONET collaboration provides globally distributed observations of spectral *AOD*, inversion products, and precipitable water in diverse aerosol regimes. Aerosol optical properties are measured at multiple wavelengths ranging from the ultraviolet to shortwave infrared. *AOD* data (accuracy: ± 0.02) are computed for three data quality levels: Level 1.0 (un-screened), Level 1.5 (cloud-screened), and Level 2.0 (cloud screened and quality-assured) (Holben et al., 1998). For comparison with PLASMA measurements, only Level 2.0 data quality for *AOD* and Angström exponent ($\alpha_{440/870}$) are used. The 2020 data from the AERONET station (St Denis) is Level 1.5. The sun-photometer we used is located on the University campus, at St Denis located in the north of the Island.

2.2.2. Microwave radiometric profiler (MWRP)

The microwave profiler RPG-HATPRO G5 gives us measurements of the microwave radiation emitted by the troposphere which provides tropospheric vertical profiles (0 – 10 km) of absolute humidity and temperature, with a special focus on the MBL. It allows to monitor with a high temporal resolution (1 min) the thermodynamic state of the atmosphere and to investigate fruitfully a wide variety of weather phenomena related to water vapour (e.g. Louf et al., 2015). A zenith-looking infrared ceilometer provides, together with the temperature profile retrieved from the MWRP, an estimate of the cloud-base height. The MWRP is also equipped with *in situ* sensors for ground level measurement of temperature, water vapour and pressure (Louf et al., 2015). It was on the University campus between December 12th, 2018 and March 11th, 2019.

2.3. Models and reanalyses

2.3.1. AROME

AROME-Indian Ocean (Bousquet et al., 2020) is used in this study in order to obtain the horizontal wind fields at different altitudes, at the places and dates where the flights were performed. This model is an adaptation of Météo-France's operational model AROME (Seity et al., 2011) to the Indian Ocean. AROME-IO has a horizontal resolution of 2.5 km and is initialized and coupled to the lateral limits by Integrated Forecasting System (Inness et al., 2013) operational analyzes (ECMWF, https://www.ecmwf.int). It is also equipped with a 1D coupling with the ocean in order to better represent the ocean-atmosphere exchanges (Bielli et al., 2021).

2.3.2. Meso-NH

Meso-NH is a non-hydrostatic mesoscale model which was developed in partnership by the Centre National de Recherches Météorologiques (CNRM) and the Laboratoire d'Aérologie (LA) and whose equations are described by Lafore et al. (1998) and Lac et al. (2018). This multidimensional model (1D, 2D or 3D) integrates a system of anelastic equations which allows simulations of a wide range of meteorological phenomena from the sub-synoptic scale (a few hundred kilometers) to the microscopic scale (a few meters). In this study, the resolution used is 500 m. Meso-NH takes into account different physical aspects such as turbulence, radiation, surface processes, microphysics … It is also coupled with gaseous, aqueous chemistry and aerosol modules which provide a privileged dynamic framework for any numerical study of atmospheric physico-chemistry.

2.3.3. FLEXPART

The FLEXPART Lagrangian Particle Dispersion Model is a comprehensive community tool for atmospheric transport modeling and analysis. It is a Lagrangian particle dispersion model that simulates the transport, diffusion, dry and wet deposition and radioactive decay of tracers released from point, line, surface or volume sources. FLEXPART can be used forward in time to simulate the dispersion of tracers from their sources, or backward in time to determine their potential source contributions (Stohl et al., 2015). In our study, FLEXPART was used to determine the back-trajectories of particles in order to know their origin. Lagrangian particle models calculate the trajectories of a large number of so-called particles (which do not necessarily represent real particles, but infinitely small patches of air) to describe the transport and diffusion of tracers in the atmosphere. FLEXPART's source code and a manual are freely available from the internet page https://www.flexpart.eu/. Recently, FLEXPART has been coupled to the Eulerian models AROME

[2] In this text, wavelengths are given with respect to the vacuum.

(Verreyken et al., 2019). In this paper, we also use a version of FLEXPART that has been coupled to meteorological output from Meso-NH.

2.3.4. CAMS reanalyses

Copernicus Atmosphere Monitoring Service (CAMS, previously MACC, https://atmosphere.copernicus.eu/) is an atmospheric model that simulates the mixing ratios of various aerosols, *AODs* or thermodynamic parameters (for example humidity, wind, temperature …) on a large scale and regional scale. The data assimilation system used for CAMS is based on the ECMWF' Integrated Forecast System (IFS). Satellite observations are implemented in this model and allow the study of the atmospheric composition (chemically reactive gases, aerosols, greenhouse gases) at global scale (Morcrette et al., 2009). CAMS allows in particular to differentiate various types of aerosols such as: (i) Sea Salt Aerosols (0.03–0.5 μm; 0.5 − 5 μm and 5 − 20 μm) and Dust aerosols (0.03 − 0.55 μm; 0.55 − 5 μm and 5 − 20 μm) divided into three size ranges, (ii) Black Carbon and Organic Matter divided into two modes (hydrophobic and hydrophylic) and (iii) Sulfate.

In our study, we use the mixing ratios of these different species (Mallet et al., 2018) as well as the *AOD*. Mixing ratios and aerosol concentrations are directly related, allowing comparison between *in-situ* measurements and CAMS data.

3. Results

3.1. From the global to local scales

Mallet et al. (2018) investigated statistically, over a 8-years period, the distribution and variability of marine aerosols in the southern Indian Ocean {10° S - 40° S; 50° E − 110° E}, by means of satellite data (POLDER and CALIOP), CAMS reanalyses, and *AOD* measurements from the AERONET sun-photometer located in St Denis (Reunion Island). They found that aerosols are mainly located below 2 km and they estimated that SSA represents 60%–80% of the total *AOD*, while sulfate and Organic Matter (OM) aerosols have low contributions.

For example, Fig. 1 shows the CAMS mixing ratios for March 22nd, 2019 at 850 hPa ($z \approx 1.5$ km). We observe, in agreement with Mallet et al. (2018), that SSA dominate the aerosol loading in the southwestern Indian Ocean region, while sulfates and OM (hydrophilic) appear in smaller amounts, and dust aerosols are negligible. The large-scale situation for this date is representative of the different days of the AEROMARINE field campaign.

Fig. 2 shows the CAMS mixing ratios η_{SSA} (for three ranges of different SSA sizes $R_{SSA} = 0.03$, 0.5, 5, and 20 µm) corresponding to the days and location of (or around) the flights of the AEROMARINE field campaign. These mixing ratios have been converted from kg/kg into a SSA number concentration #/cm^3 (Table 1) in order to better compare with further *in situ* (POPS, MAGIC and TSI) measurements. A simple enough but realistic way to perform this conversion is as follows. We first calculated the mass of SSA (in kg) for each radius R_{SSA}, $m_{SSA} = N_{SSA}\,\rho_{SSA}(4\pi R_{SSA}^3/3)$ where $\rho_{SSA} \approx 1183$ g/cm^3 is a typical mass density of SSA (Bozzo et al., 2020) and N_{SSA} is the number of SSA particles. Then, the ideal gas law gave us the volume occupied by 1 kg of dry air at standard temperature T and pressure p, *i.e.* $V = m_{air}RT/(pM)$, where $M \approx 29$ g mol^{-1} and $R \approx 8.314$ J K^{-1} mol^{-1}. Since $\eta = m_{SSA}/m_{air}$, it ensues directly $N_{SSA}/V = 3pM\,\eta_{SSA}/(4\pi R_{SSA}^3 RT\rho_{SSA})$.

The results of this conversion are summarized in Table 1. These orders of magnitude are realistic values. Another precise approach would be to consider a size distribution if it were fully available. The POPS, TSI and MAGIC size ranges of measurements (respectively 132 nm − 3 µm, < 10 nm and < 2 nm) correspond to the two smallest size ranges of the CAMS reanalyses (SSA between 0.03 μm and 5 μm). The CAMS concentrations retrieved ($SSA_{0.03-0.5\mu m}$ and $SSA_{0.5-5\mu m}$) are of the same order of magnitude as the concentrations measured by POPS, TSI and MAGIC (see Table 1). The largest SSA concentrations ($SSA_{5-20\mu m}$) are negligible compared to the other two CAMS size ranges.

We note for these flights that the SSA are not located on the same side of Reunion Island depending on the day. We will see later that this is explained by the wind regimes.

3.2. Thermodynamic parameters

Fig. 3 present the averaged profiles (for March 2019) of the relative humidity and the temperature resulting from the measurements made by the MWRP and by the CAMS reanalyses.

The radiometer and CAMS reanalysis are in agreement on the relative humidity values between 0 and 1 km, with a surface value of 70% and a maximum of 80% around 0.5–1 km in altitude. However, above 1 km, CAMS reanalyses underestimate the relative humidity from 5% at 2 km to 20% at 5 km altitude. For the temperature, CAMS reanalyses and radiometer measurements are very close to each other.

From the radiometer measurements, we observe that relative humidity varies between 50% and 100% and temperature between 283 K

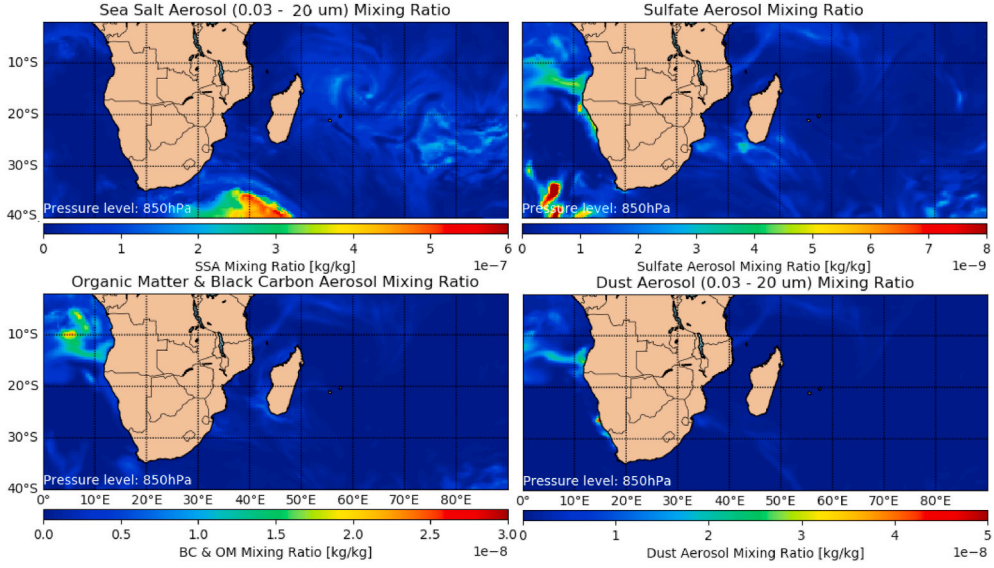

Fig. 1. CAMS reanalysis (0.25°/0.25°): mixing ratio of SSA 0.03–20 μm (top left), sulfate (top right), Organic Matter and Black Carbon (bottom left) and Dust Aerosols 0.03–20 μm (bottom right) at 850 hPa. Date: 03/22/2019 at 06:00:00 UTC.

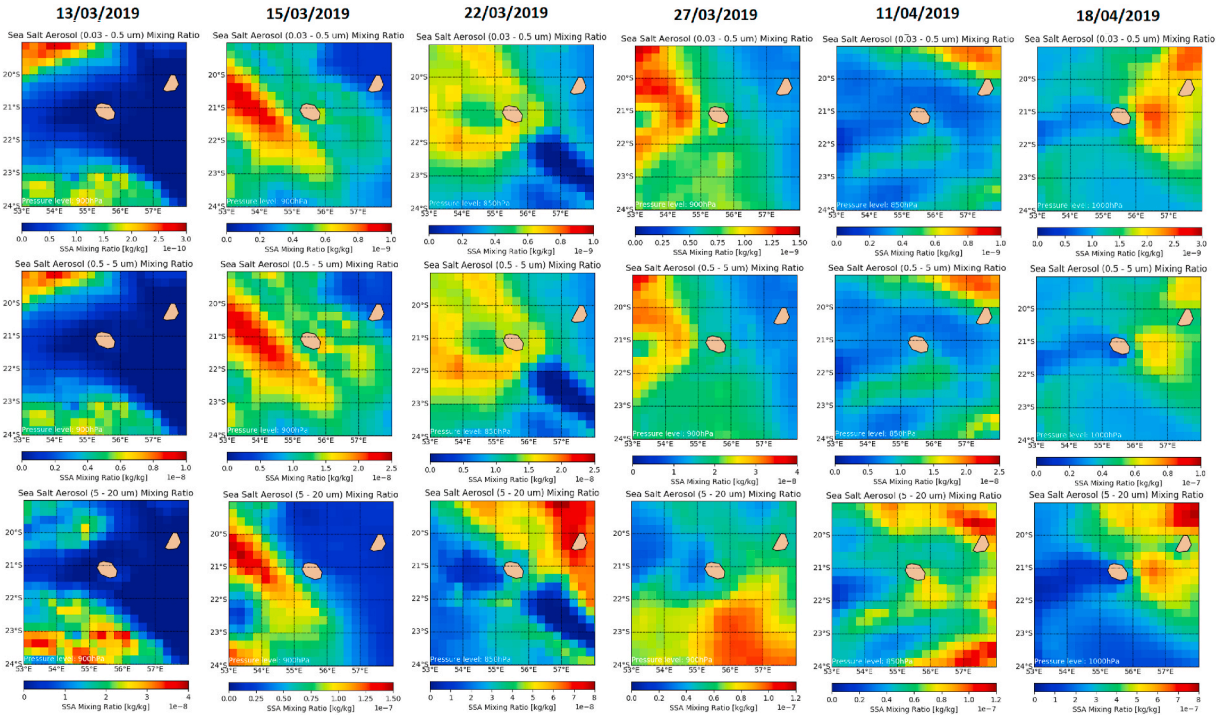

Fig. 2. CAMS reanalysis (0.25°/0.25°): mixing ratio of SSA 0.03–0.5 μm, SSA 0.5–5 μm, and SSA 5–20 μm (from top to bottom) on 03/13/2019, 03/15/2019 (at 900 hPa), 03/22/2019 (at 850 hPa), 03/27/2019 (at 900 hPa), 04/11/2019 (at 850 hPa) and 04/18/2019 (at 1000 hPa) from left to right.

Table 1
Range of concentrations measured by POPS, TSI and MAGIC and range of SSA concentrations (size ranges: 0.03–0.5 μm; 0.5 − 5 μm and 5 − 20 μm) from CAMS reanalyses in the pixel where the flight took place, for the six flight dates.

Date	MAGIC (#/cm^3)	TSI (#/cm^3)	POPS (#/cm^3)	$SSA_{0.03-0.5\mu m}$ (#/cm^3)	$SSA_{0.5-5\mu m}$ (#/cm^3)	$SSA_{5-20\mu m}$ (#/cm^3)
03/13	200 to 2.10^3	100 to 10^3	5 to 100	0.3 to $1.4.10^3$	$1.2.10^{-3}$ to 0.1	$4.6.10^{-4}$ to 0.03
03/15	200 to 300	100 to 200	50 to 100	2.3 to $1.0.10^4$	0.06 to 60	$3.7.10^{-3}$ to 0.2
03/22	–	10 to 300	32 to 100	3 to $1.3.10^4$	0.08 to 76.3	$2.8.10^{-3}$ to 0.2
03/27	500 to 2.10^3	200 to 10^3	30 to 130	4.1 to $1.9.10^4$	0.01 to 12.1	$1.8.10^{-3}$ to 0.1
04/11	800 to 8.10^3	–	74 to 130	2.4 to $1.1.10^6$	0.06 to 58.7	$5.5.10^{-3}$ to 0.4
04/18	200 to 2.10^4	–	7 to 132	6.0 to $2.7.10^4$	0.2 to 180	0.02 to 1.2

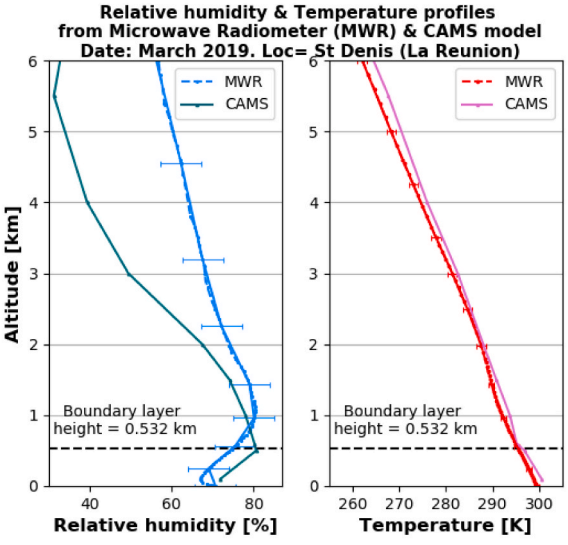

Fig. 3. Average profiles of temperature and relative humidity from microwave radiometer and from CAMS reanalysis (20.8 S; 55.2 E) for March 2019.

and 300 K in the 0 − 3 km atmospheric layer. In addition, the averaged height of the boundary layer for March 2019 is 0.532 km.

These values are representative of the thermodynamic situation during the field campaign flights. These data will be helpful to examine cloud formation under marine conditions.

3.3. *The AEROMARINE field campaign*

The AEROMARINE field campaign allowed to better understand the 3D distribution of marine aerosols around Reunion Island and how it is influenced by the dynamics of the MBL thanks to an instrumental synergy: PLASMA, POPS, Tandem CPC TSI3007 and MAGIC200 (Table 2). Six flights, of a duration of about 90 min, allowed to sample the aerosols

Table 2
Availability of instruments during flights (F1 to 6).

AVAILABLE INSTRUMENTS				
Flight	*PLASMA*	*MAGIC*	*POPS*	*TSI*
F1	✓	✓	✓	✓
F2	✓	✓	✓	✓
F3	✓	✓	✓	✓
F4	✓	✓	✓	**X**
F5	✓	✓	✓	**X**
F6	✓	✓	✓	✓

from an altitude of 100 m up to 4 km and up to about 2 km off the west coast. The flight paths are shown on Fig. 4. They were designed to have most of the time a vertical profile above the ocean, and to measure air masses above the Maïdo mountain on the way back to the airport. Since focus is put on marine aerosols, we are going to divide these flights into two groups: (I) when only the ascending part is over the ocean (F1, F2, F3) and (II) when the whole flight is over the ocean (F4, F5). Finally, flight F6 is treated separately since the plane flew over the city of St Denis (red box on Fig. 4). We will see that this flight is interesting to segregate data between land/ocean conditions.

3.3.1. Optical properties from PLASMA measurements

Fig. 5 displays the *AOD* and α vertical profiles measured by PLASMA during each flight. For group II, we have separated the ascending phase from the descending phase. For each flight and for each wavelength, the *AOD* is lower than 0.1 during the ascending phase, with values below 0.05 between 500 m and 1 km, and up to 1.5 km for flight F5. It is in agreement with other published results on marine air masses (*e.g.*, Horowitz et al., 2017) shows as multiyear daily average $AOD = 0.06 \pm 0.04$ and $\alpha = 0.7 \pm 0.36$). Higher in altitude, the *AOD* changes little with the altitude, and is constant with altitude above 2 km. It means that most of the aerosols that contribute to *AOD* (*i.e.* the largest ones) are located below 2 km, which is in agreement with previous works by Lesouëf et al. (2013) and Duflot et al. (2019).

For group II, the *AOD*-profiles during the descent differ from the ascent, especially below around 1 km of altitude, where *AODs* can reach 0.15 during the descent phase. For flight F4, the *AOD* peaks at 500 m, in particular at 500 and 650 nm. Beside the *AOD* values below 1 km altitude during the descent phase, the behaviour of the *AOD* with the wavelength does not depend on the altitude: the shortest wavelengths (380, 440 nm) show the highest *AOD*. This suggests that the sampled atmosphere was made of particles with size of the order of, or comparable to, these wavelengths, so particles rather in the accumulation mode, with the exception just mentioned which could indicate the presence of larger particles.

The Angström exponent (α) is a good qualitative indicator of the mean size of the sampled aerosols. The PLASMA measurements reveal that α is lower than 1.2, independently of the altitude. This clearly suggests the presence of marine aerosols like sea salt (Schuster et al., 2006), since the CAMS retrievals (Fig. 1) indicate that the contribution of dust aerosols were negligible. For group I, α presents in general a maximum around 1.0 within the 0.5–1.5 km layer. Regardless of local maxima in α that corresponds to sudden and localized changes in the corresponding *AOD*, the overall behaviour of α with altitude suggests that the larger particles are situated between 0.5and 1.5 km. For flight F1, α reaches a maximum of 1.5 at about 800 m in altitude, in agreement with the peak in *AOD* at 440 nm and the almost null value of *AOD* at 1 020 nm, indicating the presence of smaller particles at this altitude.

For group II, the ascent profiles share similar characteristic to those from group I with an increase of α with the altitude up to 1.5 km and a slight decrease above. The values of α vary between 0.6 and 1.2. However, larger particles seems to occupy the altitudes above 1.5 km compared to group I. Below 1.5 km, a decrease of 0.5 can be found in α values between the descent (<0.5) and ascent phases, which could indicate a depletion of small particles in favor to larger ones.

3.3.2. Aerosol concentration measurements

Fig. 6 presents the aerosol concentration measurements by MAGIC (particle size larger than 2.5 nm), TSI (particle size larger than 10 nm) and POPS (particle size larger than 132 nm). POPS concentration profiles show that the sampled particles (accumulation and coarse modes) have a maximum number concentrations of around 10^2 cm^{-3} between 0.5 and 1.5 km, and around 10 to 3×10^2 cm^{-3} above. It confirms that larger particles are found between 0.5 and 1.5 km in altitude, in

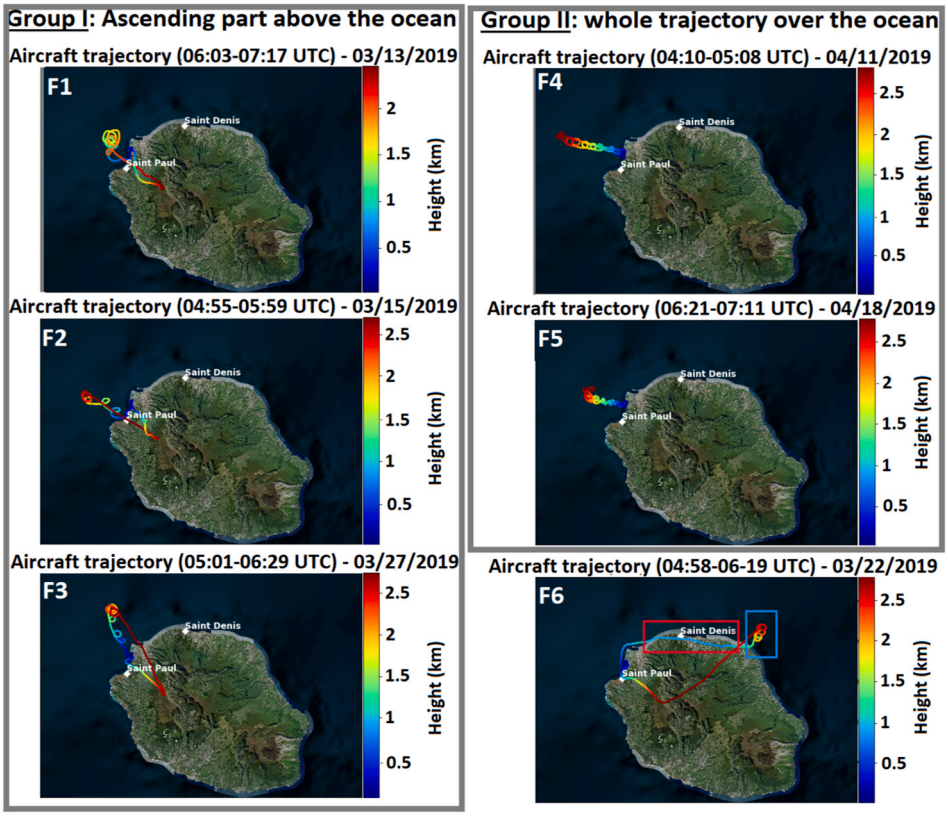

Fig. 4. Flight trajectories and altitudes on 03/13/2019, 03/15/2019, 03/27/2019 (Group I) and 04/11/2019, 04/18/2019 (Group II). The sixth flight is a particular case (see text for details).

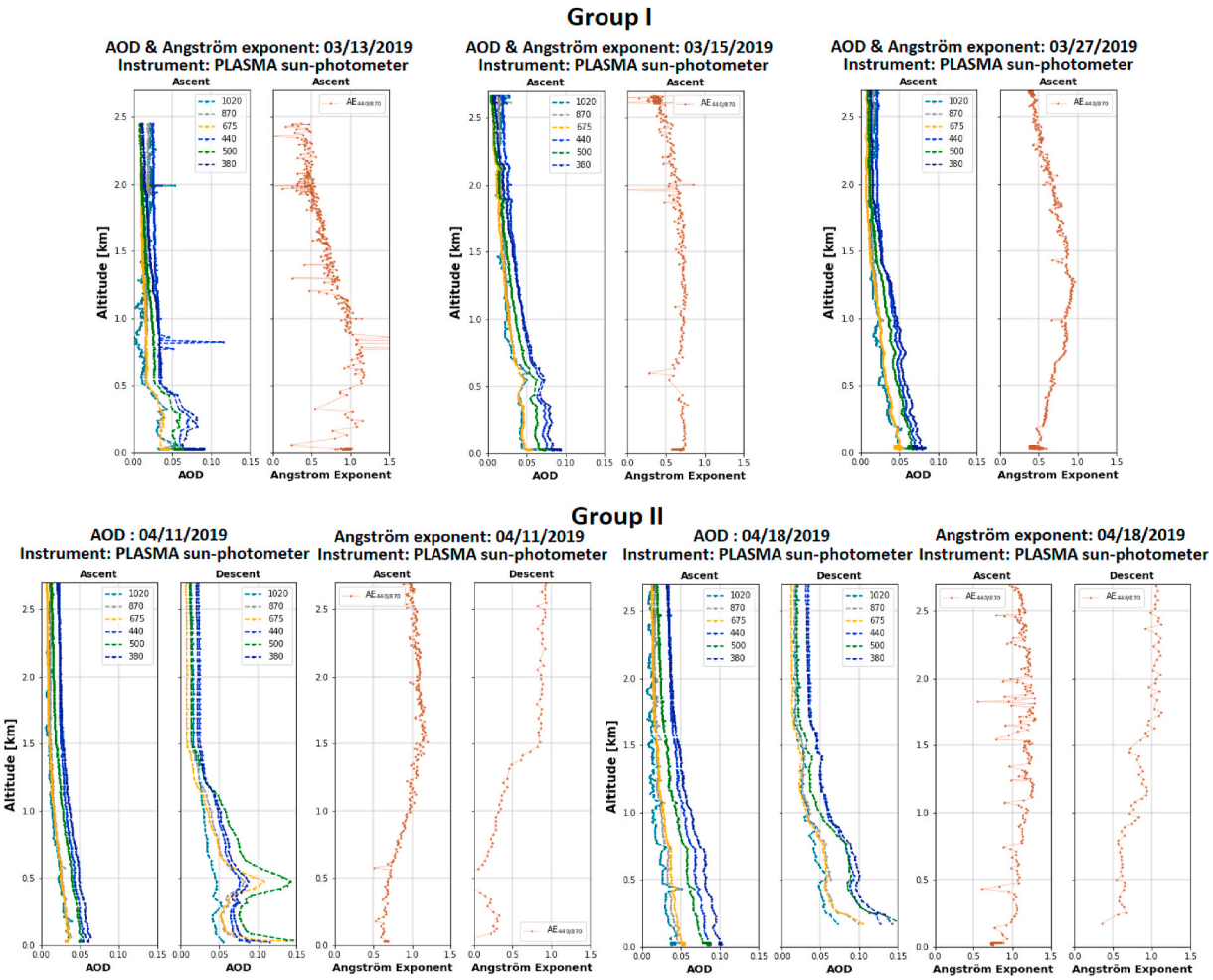

Fig. 5. *AOD* and Angström exponent (α) vertical profiles (PLASMA measurements) for flights F1, F2, F3 (Group I) and flights F4, F5 (Group II).

agreement with the conclusions deduced from the optical measurements. Below 0.5 km a.s.l, the POPS concentrations increase with altitude during the ascent phase.

The shape of the measured concentration profile can show a maximum (group I) or a minimum (group II) in the layer below 0.5 km. During the descent (group II), the POPS concentrations decrease with altitude between the surface and 0.5 km. Furthermore, the aerosols concentrations are higher between 1 and 1.5 km compared to the ascent phase, up to a factor of 10 for flight F4 at 1 km. Above 1.5 km, the POPS profiles during the ascent and descent phases are in agreement, with similar shapes and concentrations. POPS counts more particles during the descending phase of the flight. This is tempting to explain this increase by physico-chemical processes that would modify the aerosol number or the aerosol size so that small particles became large enough to be counted by POPS. However, we have to keep in mind that the trajectory of the plane during the descent is the same as the ascending trajectory, so we cannot exclude an influence of the plane in the aerosol content when coming back. Also, we cannot totally exclude that the air mass has changed by advection between the ascent and the descent of the plane.

Comparing the aerosol concentrations measured by POPS to the measurements from MAGIC and TSI will help further evaluate the vertical distribution of aerosols according to their size. Differences in TSI and MAGIC concentrations are minimum above 1.5 km. In particular, their values are almost identical above 1.5 km for flight F2, and above 2 km for flight F1. Below those altitudes, the MAGIC concentrations are around twice those of TSI. This means that small particles (nucleation mode) are twice (in concentration) than larger particles (Aïtken mode) below 1.5 km while above, there is no small particles (MAGIC-TSI ratio close to one). Such values of number concentration in the nucleation mode, between 10^3 and 10^4 cm^{-3}, have been measured also in the Mediterranean (Eleftheriadis et al., 2006).

For the flights in group I, the concentration vertical profiles obtained from MAGIC and TSI present similar shapes. On average, MAGIC concentrations are 2–3 times higher than TSI concentrations. The highest concentrations are found in the marine boundary layer below 0.7 km for flight F1, and below 0.5 km for flight F2 and F3, with values ranging from 2.10^3 to 10^4 cm^{-3}. This difference of 200 m in the marine boundary layer may be due to the fact that flight F1 occurred 1 h later in the morning compared to flights F2 and F3, so the boundary layer may have time to develop a bit more.

For flight F1, the MAGIC and TSI concentration profiles are rather constant at $2.10^2 cm^{-3}$ above 1 km. For flight F2, the concentrations are constant above 1.5 km at $4.10^2 cm^{-3}$. For flight F3, a value of $4.10^2 cm^{-3}$ is found above 2 km, and a value of $10^3 cm^{-3}$ is found in the layer between 0.8 and 1.6 km.

For group II, only MAGIC was available. Similar features can be found in the profiles of flights F4 and F5 compared to group I. Furthermore, contrary to the aerosol concentration measured by POPS, the aerosol concentrations are rather similar between the ascent and descent phases.

Other important information are obtained when comparing the POPS and MAGIC profiles. Indeed, the concentration profile differences "MAGIC - POPS" (not shown) present relatively smaller values above 0.5 km. More significant differences are obtained below this altitude. An exception occurs for flight F1 since the critical altitude is 1 km because

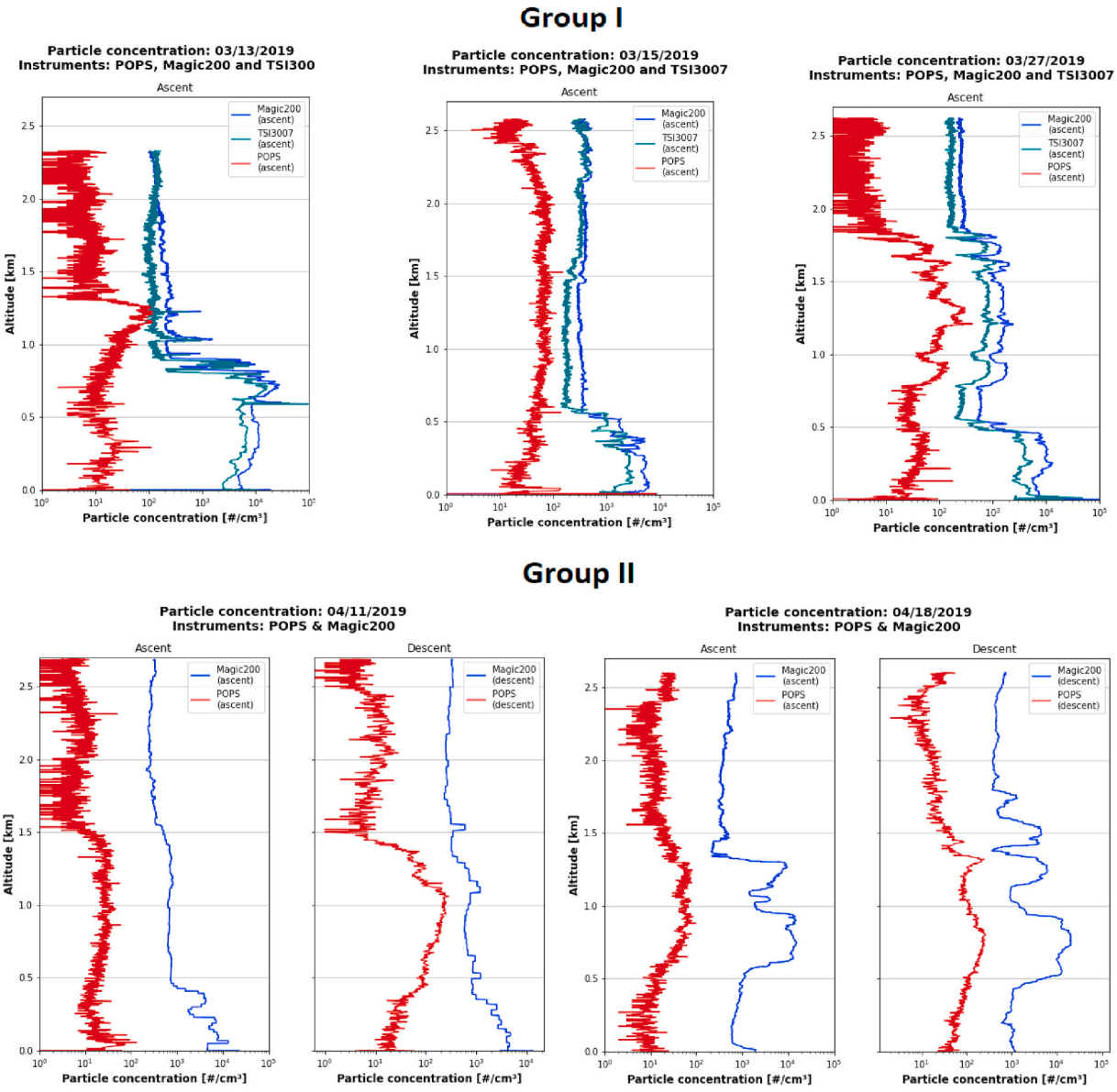

Fig. 6. Particle concentration profiles (from POPS, TSI3007 and MAGIC200 instruments) during F1, F2, F3 (Group I) and F4, F5 (Group II).

of a more developed boundary layer, as already suggested above. Another exception is for flight F5 where significant differences are between 0.5 and 1.5 km and small differences elsewhere. For group II, no significant differences are noted between the ascent and the descent *i.e.* same shape and order of magnitudes in the concentration profile differences.

In summary, the measurements indicate that the boundary layer below 0.5 km–0.7 km is much richer in aerosols in the nucleation or Aïtken modes (size lower than 132 nm). Above the boundary layer, and up to 1.5 km–2 km depending on the flight, these modes have a lower concentration and larger particles (size greater than 132 nm - accumulation mode) are dominant. The exception in the marine boundary layer for flight F5, *i.e.* below 0.5 km, means that this layer is poorer in terms of small aerosols.

3.3.3. *Origin of the air masses*

To further evaluate the origin of the air masses identified in the previous section, we used FLEXPART mesoscale backtrajectories to distinguish air masses influenced by local terrestrial emissions from those with marine origin or representative of the regional background. Here, we have chosen a backtime of 12 h because it corresponds to the domain of AROME.

tables A1 and A2 in the appendix presents statistical products from the FLEXPART output.

The scientific meaning of the FLEXPART outputs needs to be briefly reminded in order to avoid misunderstandings about the result presented in those tables. When we release an air mass at a given altitude z_r, FLEXPART is able to trace back its probable trajectories, over a geographical grid, during an user-decided time interval. From that, it is then possible to identify (and reckon) the oceanic pixels, *viz.* the trajectory grid-points located over the ocean, and similarly for the island pixels which are trajectory grid-points located over Reunion Island. In other words, we can quantify how much could the ocean contribute to, or impact, the aerosol content of the considered air mass.

Beside the geographic origin, it is possible to determine the tropospheric layer from where an air mass originates. The results from the previous sections helped us identify three layers: (L1) below 0.5 km, (L2) between 0.5 and 1.5 km, and (L3) above 1.5 km. For instance, in Table A1, the results after 12 h of backward simulations for an altitude release at 200 m for flight F1 show that 88% (first row, last column) of

the air mass originated from grid cells over the ocean, and 12% from grid cells over Reunion Island. In addition, the origin of the air mass can be analyzed in terms of geographic location and height. Hence, 43% of the air mass originated from 0 to 500 m in altitude (layer L1), 38% from 500 to 1500 m in altitude (layer L2), and 7% above 1500 m (layer L3) and above the ocean. Therefore, the origin of this air mass is mainly oceanic.

We have thus used FLEXPART to calculate the origin of air masses from different altitudes. For group I, we can see that the origin of the air masses is mainly oceanic since more than 73% of the backtrajectories originate from grid cells above the ocean.

In contrast, 28% of the air mass was located above Reunion Island, and within the layer L2 and L3. For group II, the results are different since the air masses present a significant origin above Reunion Island. In particular, the air masses released at the 200 m and 1 km altitudes for flight F4 have a dominant origin above Reunion Island.

Comparing the altitude where the backtrajectories are released, and the distribution in the vertical of the backtrajectories give additional information on the vertical transport between layers. Let us first look at oceanic pixels for group I. First, we note that the air masses with a dominant marine origin stayed, for a large part, within the same layer they originated from. For example, for a release at 200 m, 43% of the air mass with marine origin were in the layer L1. Excepted for some rare exceptions (underlined in tables), the layer that presents the highest percentages (in bold fonts in tables) includes the altitude of release. However, exchanges of air masses (in italic fonts in tables) between layers are not negligible, even if they are not dominant. For instance (flight F1), for a release at 1 km, 29% of the air mass with marine origin come from the layer L1. This means that the aerosol content in the lower troposphere is also impacted by the mixing between contiguous layers. This result holds for the air masses originating from Reunion Island, although the terrestrial component in the lower troposphere is mostly significant in the layer L2 (percentages greater than 10%). For the group II flights, we have the same results although we recognize that the insular influence is more present, especially at low level for flight F4. This may be correlated with MAGIC and PLASMA measurements. Indeed, for flight F4, the maximum MAGIC concentrations are measured below 0.5 km, which corresponds to a majority of island pixels in Table A1. It is also at this altitude that PLASMA measures the most important *AODs* (during the descending phase).

We are summarized with typical orders of magnitude the results given in Tables A1 and A2. These conclusions are summarized on Fig. 7. The vertical layering we found, and in particular the predominance of the oceanic aerosols, are explained by the interaction between the wind field and Reunion Island's complex terrain. The AROME model outputs (not shown) reveal a dominant south-west and south wind weather regime occurred over the sea at the time of the flights, with sometimes strong recirculation on the lee side, off the west coast of Reunion Island.

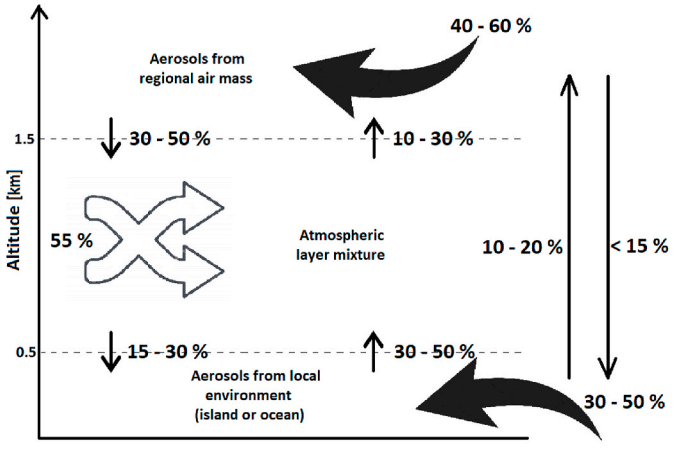

Fig. 7. Descriptive diagram of aerosols inputs and the exchanges between the atmospheric layers L1 (below 0.5 km), L2 (0.5 – 1.5 km) and L3 (above 1.5 km).

3.3.4. *Special case: flight of March 22, 2019 (F6)*

This flight (F6) is of particular interest since the plane flew over St Denis between 05:20 and 05:30UTC at an altitude of about 900 m (red box on Fig. 4), then ascended in spirals above the ocean up to 2.5 km (blue box on Fig. 4). It finally flew over St Paul before landing.

The measured *AODs* and α over St Denis (grey boxed area on Fig. 8) have a local maximum of 0.05 and minimum of 0.5 respectively, while over the ocean (blue box in Fig. 8), the measured *AODs* are constant ($AOD < 0.05$) and α is around $0.8 - 1$. This suggests that smaller particles are sampled when the plane is over St Denis.

The difference in concentration between MAGIC and POPS is much larger over St Denis than over the ocean. This means that, as indicated by the PLASMA optical measurements, small particles (size lower than 132 nm) are the dominant mode over St Denis. The MAGIC - TSI differences in concentration further indicates that the smallest particles are those that dominate. In contrary, the MAGIC - TSI difference is close to zero and confirm that larger particles are found above 1.5 km over the ocean north east of the island.

The wind direction given by AROME (not shown here) indicate (i) at 1 km (overflight of St Denis) a southeast wind of around 10 m s^{-1} coming from the island and (ii) at 1.5 km, when the plane begins these spirals above the ocean, a southeast wind from the ocean with a speed of about 8 m s^{-1}.

The FLEXPART backtrajectory results (Table A2 in the appendix section) indicate that for a release at 1.5 km, the air mass origin was purely marine and stayed above 500 m over the past 12 h. This is due to a southeasterly wind regime, according to AROME wind fields (not shown). Hence, the layer at 1.5 km in altitude is representative of the regional background.

3.4. *Comparisons with other databases*

3.4.1. *Comparison with AERONET measurements*

Assuming that the *AOD* is mostly influenced by marine aerosols on the north and west shore, one can compare *AOD* measured by the AERONET station at St Denis and the *AOD* measured by PLASMA on the runway.

Table 3 brings together the mean values of the AOD_{500nm} on the runway (before takeoff) measured by PLASMA and the AOD_{500nm} measured by the AERONET sun-photometer (St Denis) at the same time. Both the *AOD* and α from AERONET and PLASMA are in agreement for flights F2, F3 and F4. For the flight F1, the AERONET sun-photometer measures a larger Angström exponent while for flights F5 and F6 it is the *AODs* measured on the runway by PLASMA which are larger. However, these differences are consistent with the accuracy of the two photometers (AERONET: $\Delta AOD = \pm 0.02$ and PLASMA: $\Delta AOD = \pm 0.005$–0.01 according to λ). The exception of the flight over St Denis (flight F6) where $AOD_{AERONET} > AOD_{PLASMA}$ can be explained by the difference in altitude of the two measurements (0.9 km for PLASMA and ground-based for AERONET).

So AERONET measurements are generally in agreement with those carried out during flights. If one relies on the AERONET retrievals, the general agreement with the PLASMA retrievals suggests that PLASMA offered a representative sampling of the aerosol content around Reunion Island. We further evaluated this by comparing the *AOD* AERONET measurements before and during the 2020-lockdown due to the Covid19 pandemic, assuming that the terrestrial sources were similar between both periods. Reunion Island experienced a lockdown between March 17, 2020 and May 17, 2020 and hence mobile traffic and anthropogenic activities were reduced. The three plots presented in Fig. 9 show that no statistically significant change in the *AOD* or Angström exponent can be clearly attributed to the lockdown. This tends to indicate that indeed the AERONET station at St Denis is not significantly impacted by local

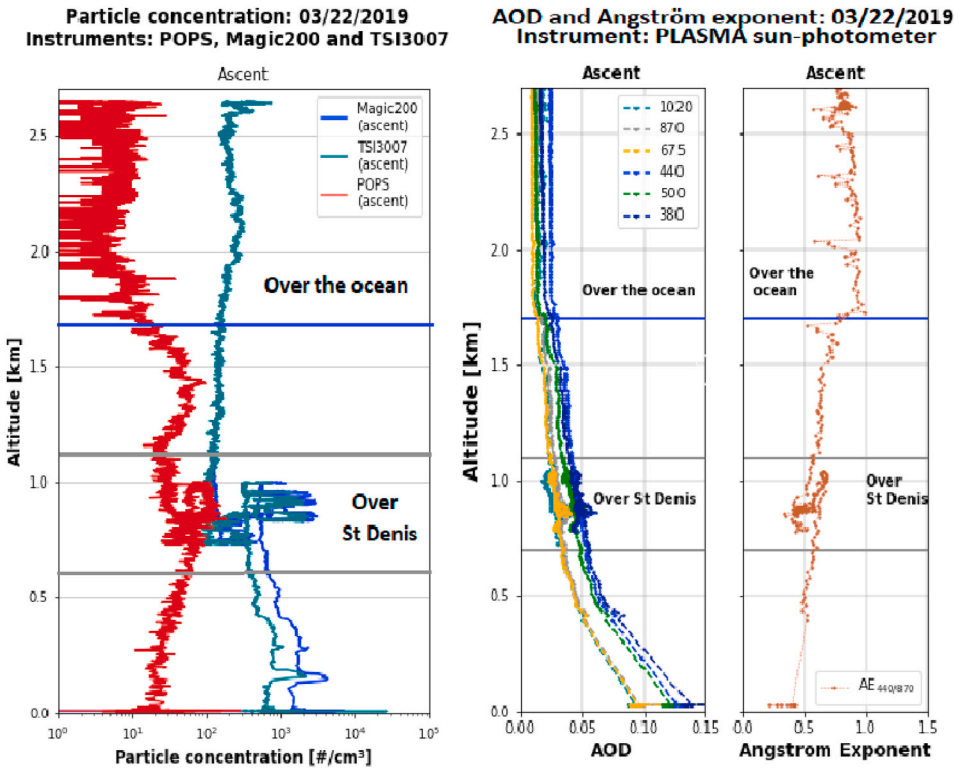

Fig. 8. Particle concentration profiles from POPS, TSI3007 and MAGIC200 instruments (left), *AOD* and Angström exponent ($\alpha_{440/870}$) profile from PLASMA sun-photometer (right) during flight on 03/22/2019 (F6).

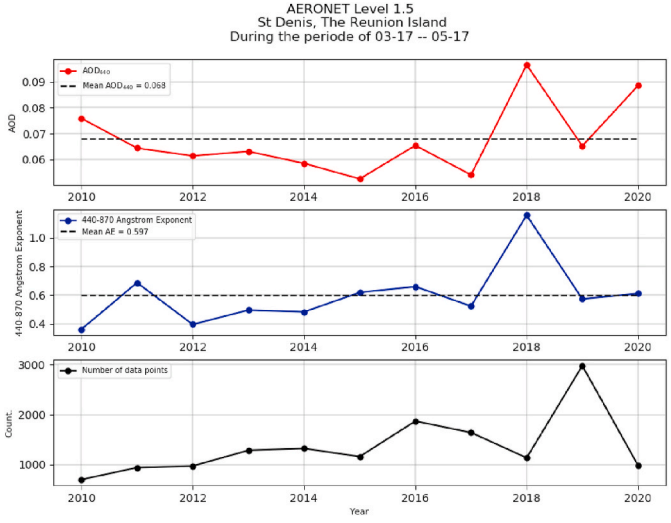

Fig. 9. Mean *AOD*, mean α and number of data points from AERONET station in St Denis (Level 1.5) for the period from March 17 to May 17 (2010–2020).

anthropogenic aerosols and confirms the results of Hamill et al. (2016) that it is a marine station.

3.4.2. Comparison with CAMS reanalyses

Fig. 10 presents the daily *AOD* averages of the CAMS model (model grid point: 20.8 S; 55.2 E) and of the AERONET sun-photometer (St Denis) for March and April 2019. Over this period, CAMS overestimates the *AOD* by 0.03.

Daily differences between CAMS reanalyses and AERONET measurements are presented in Table 4 (values rounded to the hundredth).

The monthly averages of the *AODs* given by the CAMS reanalyses is

Table 3
AOD at 500 nm and Angström exponent (α) on the runway from the PLASMA sun-photometer and from the AERONET sun-photometer (St Denis) for each flight date.

Flight	PLASMA		AERONET	
	$AOD_{500\ nm}$	α (AE)	$AOD_{500\ nm}$	α (AE)
F1	0.06	1.0	0.06	1.7
F2	0.07	0.6	0.07	0.7
F3	0.07	0.5	0.06	0.4
F4	0.05	0.6	0.04	0.7
F5	0.09	0.6	0.06	0.6
F6	0.12	0.4	0.06	0.4
Over St D.(F6)	0.04	0.5	0.07	0.2

0.11, for March and April 2019. The monthly averages of the *AODs* measured by the AERONET sun-photometer is 0.08 for March and April 2019. This shows an overestimate of CAMS of 0.03 for March and April 2019. In particular, the CAMS reanalyses overestimate the *AODs* from 0.03 to 0.09 for flights F1, F3, F4 and F6. The difference between CAMS and the AERONET sun-photometer is statistically insignificant for flights F2 and F5.

These results agree with those obtained by Mallet et al. (2018) who determined that the *AODs* given by CAMS overestimate by about 0.05 the local AERONET measurements.

3.4.3. Comparison with Maïdo measurements

The *in situ* measurements on board the light plane in the free troposphere are further compared to the measurements from the high altitude Maïdo Observatory (21.08° S, 55.38° E; 2.2 km). We use the measurements made by a Scanotron particle counter described in Foucart et al. (2018) (concerning aerosols of size 10 − 600 nm) and a CPC TSI (aerosols greater than 10 nm) from the Maïdo Observatory for comparison with the in-flight data (POPS, TSI and MAGIC). Due to a complex interplay between land-sea breeze, catabatic wind and complex

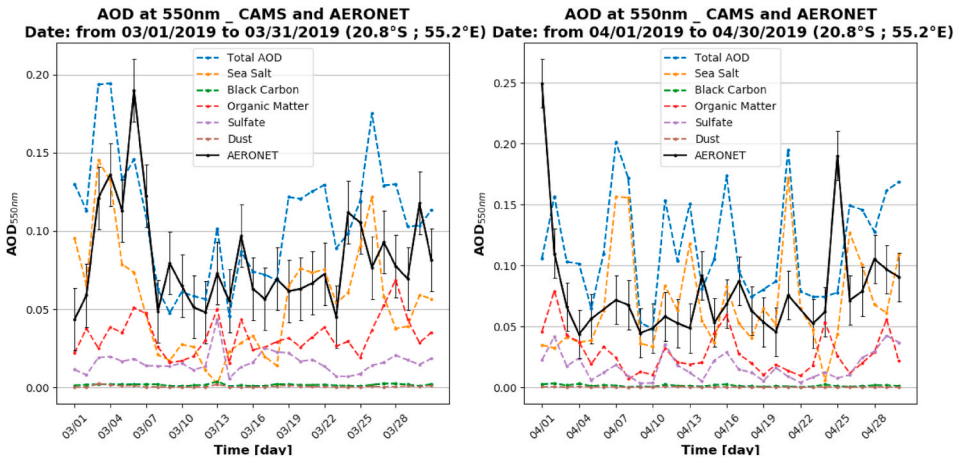

Fig. 10. *AOD* measurements from AERONET sun-photometer (Level 1.5) and from CAMS reanalysis (20.8 S; 55.2 E) for March 2019 and April 2019.

Table 4
Differences in daily *AOD* averages of the CAMS model (20.8 S; 55.2 E) and of the AERONET sun-photometer (St Denis) for each flight.

Flight	AOD_{CAMS}-$AOD_{AERONET}$
F1	+0.03
F2	- 0.01
F3	+0.04
F4	+0.09
F5	+0.01
F6	+0.06

terrain, only the in-situ measurements Maïdo taken between 21:00 and 03:00 UTC can be considered as free tropospheric (Verreyken et al., 2021).

Fig. 11 display the mensual averages for March and April 2018 for the Scanotron and the TSI located at Maïdo. The time series (POPS, TSI and MAGIC measurements) during the flights of March 22, 2019 and April 11, 2019 are also presented for comparison.

For March, the average TSI measurements at Maïdo and during the flight have the same order of magnitude concentrations (between 40 and 4.10^3#.cm^{-3}). However, the POPS measurements during the flight (March and April) are much lower than those of the Scanotron at 2.2 km. The Scanotron (10 − 600 nm) measures aerosols smaller than the POPS (132 nm - 3 μm). This would mean that the majority of the aerosols measured above 2.2 km are less than 132 nm (in agreement with CAMS section 3.1).

Table 5 presents the measurements made during flights in the free troposphere (measurements for an altitude higher than 2 km) and the average concentrations measured at the Maïdo Observatory (2.2 km) during the nights before and after the flights, when the observatory is in the free troposphere.

Overall, the MAGIC and TSI measurements made during flight in the free troposphere are of the same order of magnitude as the Scanotron night measurements made at the Maïdo Observatory, in the free troposphere (between 1×10^2 and 7×10^2cm^{-3}). The two TSI CPCs (at the Maïdo Observatory and on the plane) also measure identical concentrations above 2 km (around 10^2 cm^{-3}).

We can conclude that the night-time measurements at the Maïdo Observatory (at 2.2 km) are representative of the daytime measurements (during flights) in the free troposphere and allow sampling of purely marine aerosols.

4. Conclusion

In this paper, we have presented the AEROMARINE field campaign which took place between February and April 2019 off the coast of Reunion Island (southwestern Indian Ocean). This area, identified as a pristine region, is of major interest for the study of marine aerosols, their vertical distribution and their optical properties.

During this campaign, a MWRP was deployed in St Denis (93 m in the north of the Island) between mid-December 2018 and mid-March 2019. This made it possible to determine that, during the austral summer in this region, the thermodynamic situation (humidity, temperature, and height of the boundary layer) is relatively stable.

In addition, six instrumented flights allowed the aerosols to be sampled from an altitude of 100 m up to 4 km by spiraling above the ocean thanks to an instrumental synergy.

The optical properties of the aerosols were measured by the PLASMA photometer and three particle counters (POPS, TSI and MAGIC) measured the aerosol concentrations for different size ranges (accumulation, coarse and Aïtken modes). POPS analysis indicates that almost all of the particles are in the accumulation mode, centered around a particle size of 132 nm.

The results obtained show *AODs* less than 0.1 (with some exceptions), which is representative of a pristine region. The various measurements (*AOD*, Angström exponents, and concentrations) also indicate that the aerosols are in the accumulation and coarse modes, and mainly below 2 km of altitude.

The FLEXPART simulations enabled to determine the most probable origin of the aerosols measured during the flights. As a result, the aerosols follow the following vertical distribution:

- Above an altitude of 1.5 km, the sampled aerosols are not substantially impacted by the surface (layer L1 has a relatively little contribution). This is interesting since it allows to quantify the background aerosol concentration. For all the flights, we have estimated that the number concentrations (in cm^{-3}) are 300 (MAGIC), 230 (TSI) and 15 (POPS). Also, the assessed AOD_{550nm} and α are respectively 0.01 and 0.75.
- Below 0.5 km (in the MBL), aerosols come essentially from the surface. The origin can be oceanic (33%) or insular (8%). Insular influence are nonetheless due to special events depending on the wind regime (*e.g.*, the Cap La Houssaye may bring sometimes dust aerosols).
- The intermediate layer, *i.e.* between 1.5 and 0.5 km, is a layer of mixture: aerosols are mixed with those coming from the lower or upper atmospheric layers.

These results meet the initial objectives of the AEROMARINE campaign: (i) to characterize marine aerosol optical properties and their vertical distribution and (ii) to examine the transport pathways of

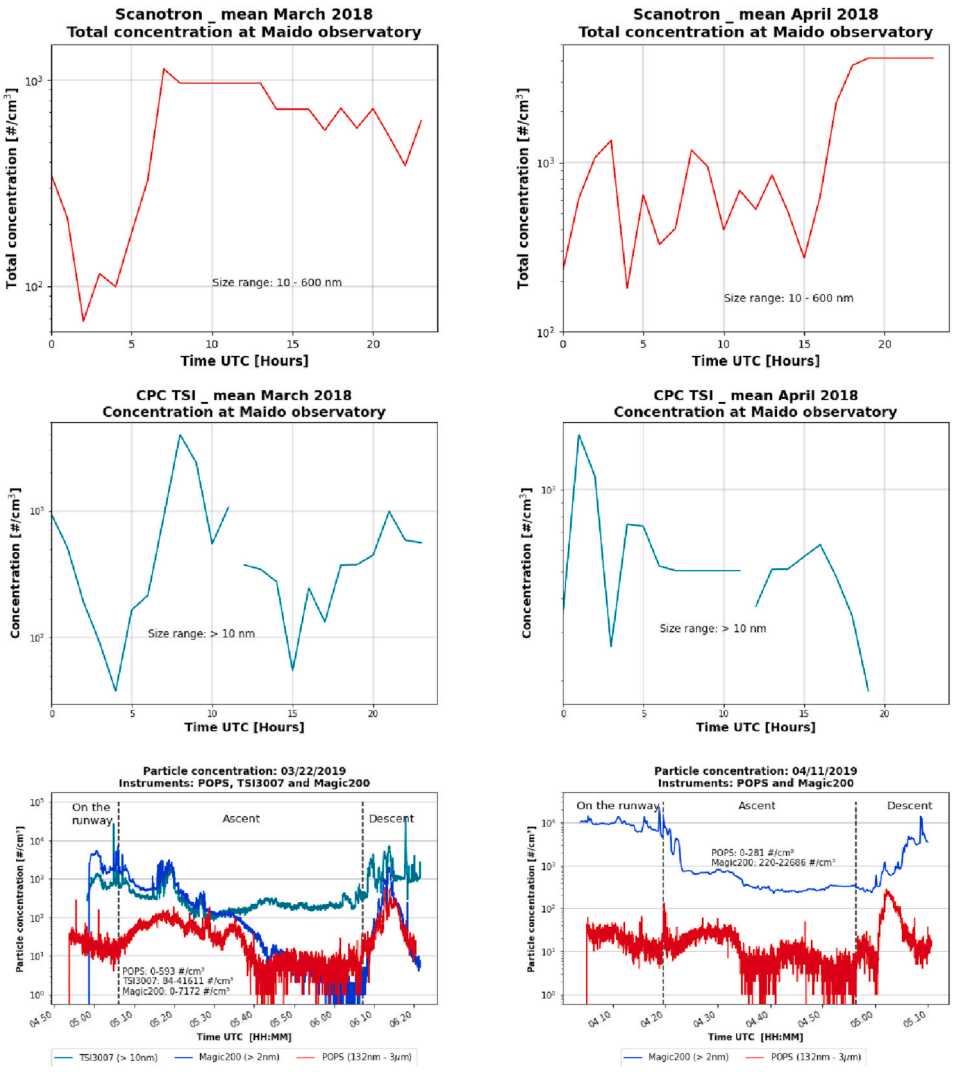

Fig. 11. March and April 2018 averages of measurements at the Maïdo Observatory by the Scanotron and the CPC TSI and time series of concentrations measured during the flights of 03/22/2019 (F6) and 04/11/2019 (F4).

Table 5
Comparison of average night-time concentrations (Maïdo Observatory) and concentrations in the free troposphere during flights.

Date	Mean night-time concentration at Maïdo D-1 (21:00–03:00 UTC)		Concentrations during flights (in free troposphere)			Mean night-time concentration at Maïdo D+1 (21:00–03:00 UTC)	
	Scanotron (#/cm^3)	TSI (#/cm^3)	POPS (#/cm^3)	TSI (#/cm^3)	MAGIC (#/cm^3)	Scanotron (#/cm^3)	TSI (#/cm^3)
03/13	130	**X**	0–21	102–180	101–146	**X**	**X**
03/15	190	**X**	3–97	226–542	244–542	211	247
03/22	321	**X**	0–29	147–746	**X**	143	**X**
03/27	268	**X**	0–12	126–221	213–302	191	**X**
04/11	129	376	0–50	**X**	236–347	110	347
04/18	**X**	549	1–54	**X**	379–771	**X**	671

marine aerosols from the MBL to the free troposphere. It is worth mentioning that the flights were carried out between 04:00 and 07:00 UTC, *viz.* during the transient convection regime between nocturnal and diurnal conditions. Further observational studies and field campaign may be necessary to examine aerosol distributions during purely diurnal and nocturnal regimes, *i.e.* for well established regimes. The AERO-MARINE campaign presented here is interesting in the sense that it documents a transient regime, namely a more complex regime in terms of thermodynamics compared to established ones.

The measurements taken during the flights were compared with the CAMS reanalyses. They showed that, like in-flight measurements, SSAs are predominant around Reunion Island and that aerosols are mainly located below 2 km. It was also shown that CAMS overestimates the *AODs* (from 0.01 to 0.09) in this region in agreement with results from Mallet et al. (2018). In addition, a comparison between PLASMA measurements (on the runway) and the AERONET sun-photometer (located in St Denis) as well as a study on the impact of 2020-lockdown due to the Covid-19 pandemic on AERONET measurements were carried out. The results strongly suggested that the AERONET station is a marine station. In other words, measurements are not impacted by local anthropogenic

activities and the station can be considered as representative of marine conditions. The AEROMARINE campaign occurred around Reunion Island. Another field campaign, the Marion Dufresne Atmospheric Program - Indian Ocean (MAP-IO), aboard the Marion Dufresne around the Terres Australes Françaises (TAF) is planned for January 2021. Among the objectives, one of them is to better document the exchanges between the pristine Southern Indian Ocean and the atmosphere. For our topic, this campaign will allow the results presented in this paper to be deepened, since it will provide data about marine aerosol emissions and of aerosol and humidity exchanges between the pristine ocean and the MBL far from any land. All of these data (from AEROMARINE and then MAP-IO) will be helpful to feed models of water vapour-aerosols-clouds interactions (Pujol and Jensen, 2019). Such features will be the topic of future research.

Declaration of competing interest

The authors declare that they have no known competing financial interests or personal relationships that could have appeared to influence the work reported in this paper.

Acknowledgements

This work was supported by the French national programme LEFE/INSU. We are grateful to the Labex CAPPA (ANR-11-LABX-0005-01) which has funded this work in the context of the Cloud-aerosol interactions work package. We acknowledge the ECMWF for providing freely reanalysis.

Appendix. FLEXPART simulations. Flights: F1, F2, F3 and F4

Table A1
Origin of air masses for L1, L2 and L3 according to a 12 h-simulation of the FLEXPART model for F1, F2, F3 and F4.

Group I: F1 and F2

FLEXPART simulation. Flight: F1. 12 h-simulation					FLEXPART simulation. Flight: F2. 12 h-simulation				
Altitude	**0–500 m**	**500–1500 m**	**> 1500 m**	**Total**	**Altitude**	**0–500 m**	**500–1500 m**	**> 1500 m**	**Total**
Altitude release: 200 m					**Altitude release: 200 m**				
Ocean	**43%**	*38%*	7%	88%	**Ocean**	**25%**	*44%*	24%	93%
Island	2%	*6%*	4%	12%	**Island**	3%	*3%*	0.0%	7%
Altitude release: 1000 m					**Altitude release: 1000 m**				
Ocean	*29%*	**37%**	11%	77%	**Ocean**	14%	**51%**	*33%*	98%
Island	4%	**17%**	2%	23%	**Island**	0	0	0	0
Altitude release: 1500 m					**Altitude release: 1500 m**				
Ocean	13%	*29%*	**31%**	73%	**Ocean**	2%	*37%*	**61%**	100%
Island	3%	*19%*	15%	27%	**Island**	0	0	0	0

Group II: F4 and F5

FLEXPART simulation. Flight: F4. 12 h-simulation					FLEXPART simulation. Flight: F5. 12 h-simulation				
Altitude	0–500 m	500–1500 m	>1500 m	Total	Altitude	0–500 m	500–1500 m	>1500 m	Total
Altitude release: 200 m					**Altitude release: 200 m**				
Ocean	**23%**	*15%*	4%	43%	Ocean	**33%**	*28%*	6%	67%
Island	**28%**	*21%*	8%	57%	Island	4%	*14%*	*13%*	33%
Altitude release: 1000 m					**Altitude release: 1000 m**				
Ocean	7%	**21%**	*11%*	39%	Ocean	*12%*	**27%**	*11%*	50%
Island	*18%*	**33%**	*10%*	61%	Island	6%	**31%**	*13%*	50%
Altitude release: 1500 m					**Altitude release: 1500 m**				
Ocean	1%	*20%*	**20%**	61%	Ocean	1%	*15%*	**23%**	41%
Island	0	22%	*17%*	39%	Island	5%	27%	*24%*	59%

FLEXPART simulation. Flights: F3 and F6

Table A2
Same as Table A1 but for F3 and F6.

F3 (Group I) and F6				
FLEXPART simulation. Flight: F3				
Altitude	**0–500 m**	**500–1500 m**	**> 1500 m**	**Total**
Altitude release: 200 m				
Ocean	**43%**	*38%*	15%	96%
Island	**2%**	1%	1%	4%
Altitude release: 1000 m				
Ocean	*19%*	**42%**	*27%*	88%
Island	2%	**7%**	*4%*	12%
Altitude release: 1500 m				
Ocean	8%	41%	*39%*	88%
Island	2%	8%	3%	13%
FLEXPART simulation. Flight: F6 12h-simulation				
Altitude release: 1500 m				
Ocean	0.0%	*35%*	**65%**	100%
Island	0.0%	0.0%	0.0%	0.0%

References

Andreae, M., Rosenfeld, D., 2008. Aerosol–cloud–precipitation interactions. part 1. the nature and sources of cloud-active aerosols. Earth Sci. Rev. 89, 13–41.

AngstrÖm, A., 1961. Techniques of determinig the turbidity of the atmosphere. Tellus 13, 214–223. https://doi.org/10.3402/tellusa.v13i2.9493.

Baray, J.L., Courcoux, Y., Keckhut, P., Portafaix, T., Tulet, P., Cammas, J.P., Hauchecorne, A., Godin-Beekmann, S., De Mazière, M., Hermans, C., Desmet, F., Sellegri, K., Colomb, A., Ramonet, M., Sciare, J., Vuillemin, C., Hoareau, C., Dionisi, D., Duflot, V., Vérèmes, H., Porteneuve, J., Gabarrot, F., Gaudo, T., Metzger, J.M., Payen, G., Leclair De Bellevue, J., Barthe, C., Posny, F., Abchiche, A., Delmas, R., Ricaud, P., 2013. Maïdo observatory: a new high-altitude station facility at Reunion Island (21° S, 55° E) for long-term atmospheric remote sensing and in situ measurements. Atmospheric Measurement Techniques 6, 2865–2877. https://doi.org/10.5194/amt-6-2865-2013.

Bielli, S., Barthe, C., Bousquet, O., Tulet, P., Pianezze, J., 2021. The effect of atmosphere-ocean coupling on the structure and intensity of tropical cyclone bejisa in the southwest indian ocean. Atmosphere 12. https://doi.org/10.3390/atmos12060688.

Bousquet, O., Barbary, D., Bielli, S., Kebir, ., Raynaud, L., Malardel, S., Faure, G., 2020. An evaluation of tropical cyclone forecast in the southwest indian ocean basin with arome-indian ocean convection-permitting numerical weather predicting system. Atmos. Sci. Lett. 21, e950 https://doi.org/10.1002/asl.950.

Bozzo, A., Benedetti, A., Flemming, J., Kipling, Z., Rémy, S., 2020. An aerosol climatology for global models based on the tropospheric aerosol scheme in the integrated forecasting system of ecmwf. Geosci. Model Dev. (GMD) 13, 1007–1034. https://doi.org/10.5194/gmd-13-1007-2020.

Crumeyrolle, S., Manninen, H.E., Sellegri, K., Roberts, G., Gomes, L., Kulmala, M., Weigel, R., Laj, P., Schwarzenboeck, A., 2010. New particle formation events measured on board the ATR-42 aircraft during the EUCAARI campaign. Atmos. Chem. Phys. 10, 6721–6735. https://doi.org/10.5194/acp-10-6721-2010.

Duflot, V., Tulet, P., Flores, O., Barthe, C., Colomb, A., Deguillaume, L., Vaïtilingom, M., Perring, A., Huffman, A., Hernandez, M.T., Sellegri, K., Robinson, E., O'Connor, D.J., Gomez, O.M., Burnet, F., Bourrianne, T., Strasberg, D., Rocco, M., Bertram, A.K., Chazette, P., Totems, J., Fournel, J., Stamenoff, P., Metzger, J.M., Chabasset, M., Rousseau, C., Bourrianne, E., Sancelme, M., Delort, A.M., Wegener, R.E., Chou, C., Elizondo, P., 2019. Preliminary results from the farce 2015 campaign: multidisciplinary study of the forest–gas–aerosol–cloud system on the tropical island of la réunion. Atmos. Chem. Phys. 19, 10591–10618. https://doi.org/10.5194/acp-19-10591-2019.

Eleftheriadis, K., Colbeck, I., Housiadas, C., Lazaridis, M., Mihalopoulos, N., Mitsakou, C., Smolík, J., Ždímal, V., 2006. Size distribution, composition and origin of the submicron aerosol in the marine boundary layer during the eastern mediterranean "sub-aero" experiment. Atmos. Environ. 40, 6245–6260. https://doi.org/10.1016/j.atmosenv.2006.03.059.

Foucart, B., Sellegri, K., Tulet, P., Rose, C., Metzger, J.M., Picard, D., 2018. High occurrence of new particle formation events at the maïdo high-altitude observatory (2150 m), réunion (indian ocean). Atmos. Chem. Phys. 18, 9243–9261. https://doi.org/10.5194/acp-18-9243-2018.

Gantt, B., Meskhidze, N., 2013. The physical and chemical characteristics of marine primary organic aerosol: a review. Atmos. Chem. Phys. 13, 3979–3996.

Gao, R.S., Telg, H., McLaughlin, R.J., Ciciora, S.J., Watts, L.A., Richardson, M.S., Schwarz, J.P., Perring, A.E., Thornberry, T.D., Rollins, A.W., Markovic, M.Z., Bates, T.S., Johnson, J.E., Fahey, D.W., 2016. A light-weight, high-sensitivity particle spectrometer for pm2.5 aerosol measurements. Aerosol. Sci. Technol. 50, 88–99. https://doi.org/10.1080/02786826.2015.1131809.

Guilpart, E., Vimeux, F., Evan, S., Brioude, J., Metzger, J.M., Barthe, C., Risi, C., Cattani, O., 2017. The isotopic composition of near-surface water vapor at the maïdo observatory (reunion island, southwestern indian ocean) documents the controls of the humidity of the subtropical troposphere. J. Geophys. Res.: Atmosphere 122, 9628–9650. https://doi.org/10.1002/2017JD026791.

Hamill, P., Giordano, M., Ward, C., Giles, D., Holben, B., 2016. An aeronet-based aerosol classification using the mahalanobis distance. Atmos. Environ. 140, 213–233. https://doi.org/10.1016/j.atmosenv.2016.06.002.

Holben, B., Eck, T., Slutsker, I., Tanré, D., Buis, J., Setzer, A., Vermote, E., Reagan, J., Kaufman, Y., Nakajima, T., Lavenu, F., Jankowiak, I., Smirnov, A., 1998. Aeronet—a federated instrument network and data archive for aerosol characterization. Rem. Sens. Environ. 66, 1–16. https://doi.org/10.1016/S0034-4257(98)00031-5.

Horowitz, Hannah M., Garland, Rebecca M., Thatcher, Marcus, Landman, Willem A., Dedekind, Zane, van der Merwe, Jacobus, Engelbrecht, Francois A., 2017. Evaluation of climate model aerosol seasonal and spatial variability over Africa using AERONET. Atmos. Chem. Phys. 17, 13999–14023. https://doi.org/10.5194/acp-17-13999-2017.

Inness, A., Baier, F., Benedetti, A., Bouarar, I., Chabrillat, S., Clark, H., Clerbaux, C., Coheur, P., Engelen, R.J., Errera, Q., Flemming, J., George, M., Granier, C., Hadji-Lazaro, J., Huijnen, V., Hurtmans, D., Jones, L., Kaiser, J.W., Kapsomenakis, J., Lefever, K., Leitão, J., Razinger, M., Richter, A., Schultz, M.G., Simmons, A.J., Suttie, M., Stein, O., Thépaut, J.N., Thouret, V., Vrekoussis, M., Zerefos, C., 2013. The MACC reanalysis: an 8 yr data set of atmospheric composition. Atmos. Chem. Phys. 13, 4073–4109. https://doi.org/10.5194/acp-13-4073-2013.

Karol, Y., Tanré, D., Goloub, P., Vervaerde, C., Balois, J.Y., Blarel, L., Podvin, T., Mortier, A., Chaikovsky, A., 2013. Airborne sun photometer plasma: concept, measurements, comparison of aerosol extinction vertical profile with lidar. Atmospheric Measurement Techniques 6. https://doi.org/10.5194/amt-6-2383-2013.

Koren, I., Dagan, G., Altaratz, O., 2014. From aerosol-limited to invigoration of warm convective clouds. Science 344, 1143–1146. https://doi.org/10.1126/science.1252595.

Kusmierczyk-Michulec, J., de Leeuw, G., Gonzalez, C.R., 2002. Empirical relationships between aerosol mass concentrations and Ångström parameter. Geophys. Res. Lett. 29 (49), 1–49. https://doi.org/10.1029/2001GL014128, 4.

Lac, C., Chaboureau, J.P., Masson, V., Pinty, J.P., Tulet, P., Escobar, J., Leriche, M., Barthe, C., Aouizerats, B., Augros, C., Aumond, P., Auguste, F., Bechtold, P., Berthet, S., Bielli, S., Bosseur, F., Caumont, O., Cohard, J.M., Colin, J., Couvreux, F., Cuxart, J., Delautier, G., Dauhut, T., Ducrocq, V., Filippi, J.B., Gazen, D., Geoffroy, O., Gheusi, F., Honnert, R., Lafore, J.P., Lebeaupin Brossier, C., Libois, Q., Lunet, T., Mari, C., Maric, T., Mascart, P., Mogé, M., Molinié, G., Nuissier, O., Pantillon, F., Peyrillé, P., Pergaud, J., Perraud, E., Pianezze, J., Redelsperger, J.L., Ricard, D., Richard, E., Riette, S., Rodier, Q., Schoetter, R., Seyfried, L., Stein, J., Suhre, K., Taufour, M., Thouron, O., Turner, S., Verrelle, A., Vié, B., Visentin, F., Vionnet, V., Wautelet, P., 2018. Overview of the meso-nh model version 5.4 and its applications. Geosci. Model Dev. (GMD) 11, 1929. https://doi.org/10.5194/gmd-11-1929-2018.

Lafore, J.P., Stein, J., Asencio, N., Bougeault, P., Ducrocq, V., Duron, J., Fischer, C., Héreil, P., Mascart, P., Masson, V., Pinty, J.P., Redelsperger, J.L., Richard, E., Vilà-Guerau de Arellano, J., 1998. The meso-nh atmospheric simulation system. part i: adiabatic formulation and control simulations. Ann. Geophys. 16, 90–109. https://doi.org/10.1007/s00585-997-0090-6.

Lesouëf, D., Gheusi, F., Chazette, P., Delmas, R., Sanak, J., 2013. Low tropospheric layers over reunion island in lidar-derived observations and a high-resolution model. Boundary-Layer Meteorol. 149, 425–453. https://doi.org/10.1007/s10546-013-9851-9.

Louf, V., Pujol, O., Sauvageot, H., Riédi, J., 2015. Seasonal and diurnal water vapour distribution in the sahelian area from microwave radiometric profiling observations. Q. J. R. Meteorol. Soc. 141, 2643–2653. https://doi.org/10.1002/qj.2550.

Luo, T., Yuan, R., Wang, Z., 2014. On factors controlling marine boundary layer aerosol optical depth. J. Geophys. Res.: Atmosphere 119, 3321–3334. https://doi.org/10.1002/2013JD020936.

Mallet, P.E., Pujol, O., Brioude, J., Evan, S., Jensen, A., 2018. Marine aerosol distribution and variability over the pristine southern indian ocean. Atmos. Environ. 182, 17–30. https://doi.org/10.1016/j.atmosenv.2018.03.016.

Morcrette, J.J., Boucher, O., Jones, L., Salmond, D., Bechtold, P., Beljaars, A., Benedetti, A., Bonet, A., Kaiser, J.W., Razinger, M., Schulz, M., Serrar, S., Simmons, A.J., Sofiev, M., Suttie, M., Tompkins, A.M., Untch, A., 2009. Aerosol analysis and forecast in the european centre for medium-range weather forecasts integrated forecast system: forward modeling. J. Geophys. Res.: Atmosphere 114. https://doi.org/10.1029/2008JD011235.

Myhre, G., Shindell, D., Bréon, F.M., Collins, W., Fuglestvedt, J., Huang, J., Koch, D., Lamarque, J.F., Lee, D., Mendoza, B., Nakajima, T., Robock, A., Stephens, G., Takemura, T., Zhang, H., 2013. Anthropogenic and Natural Radiative Forcing. Cambridge University Press, Cambridge, United Kingdom and New York, NY, USA, pp. 659–740. https://doi.org/10.1017/CBO9781107415324.018 book section 8.

O'Dowd, C.D., de Leeuw, G., 2007. Marine aerosol production: a review of the current knowledge. Phil. Trans. Math. Phys. Eng. Sci. 365, 1753–1774. https://doi.org/10.1098/rsta.2007.2043.

Pant, V., Deshpande, C., Kamra, A., 2009. The concentration and number size distribution measurements of the marine boundary layer aerosols over the indian ocean. Atmos. Res. 92, 381–393. https://doi.org/10.1016/j.atmosres.2008.12.004.

Popovici, I., Goloub, P., Mortier, A., Podvin, T., Blarel, L., Loisil, R., Deroo, C., Victori, S., Torres, B., Unga, F., Choël, M., 2018. Un système mobile pour l'étude de la distribution verticale des aérosols dans l'atmosphère : description et premiers résultats. Pollut. Atmos. https://doi.org/10.4267/pollution-atmospherique.6510 [Online] 236.

Pujol, Olivier, Jensen, Andrew, 2019. Cloud–rain predator–prey interactions: Analyzing some properties of the Koren–Feingold model and introduction of a new species-competition bulk system with a Hopf bifurcation. Phys. Nonlinear Phenom. 399, 86–94.

Ramachandran, S., 2004. Spectral aerosol optical characteristics during the northeast monsoon over the arabian sea and the tropical indian ocean: 1. aerosol optical depths and their variabilities. J. Geophys. Res.: Atmosphere 109. https://doi.org/10.1029/2003JD004476.

Schuster, G.L., Dubovik, O., Holben, B.N., 2006. Angstrom exponent and bimodal aerosol size distributions. Journal of Geophysical Research - Atmospheres 111.

Schwier, A., Sellegri, K., Mas, S., Charrière, B., Pey, J., Rose, C., Temime-Roussel, B., Jaffrezo, J.L., Parin, D., Picard, D., Ribeiro, M., Roberts, G., Sempere, R., Marchand, N., D'Anna, B., 2017. Primary marine aerosol physical flux and chemical composition during a nutrient enrichment experiment in mesocosms in the Mediterranean Sea. Atmos. Chem. Phys. 17, 14645–14660. https://doi.org/10.5194/acp-17-14645-2017.

Seity, Y., Brousseau, P., Malardel, S., Hello, G., Bénard, P., Bouttier, F., Lac, C., Masson, V., 2011. The arome-France convective-scale operational model. Mon. Weather Rev. 139, 976–991.

Stohl, A., Sodemann, H., Eckhardt, S., Frank, A., Seibert, P., Wotawa, G., 2015. The Lagrangian particle dispersion model flexpart version 8.2. https://www.flexpart.eu/wiki/FpDocumentation.

Verreyken, B., Amelynck, C., Schoon, N., Müller, J.F., Brioude, J., Kumps, N., Hermans, C., Metzger, J.M., Stavrakou, T., 2021. Measurement report: source apportionment of volatile organic compounds at the remote high-altitude maïdo observatory. Atmospheric Chemistry and Physics Discussions 2021 1–37. https://doi.org/10.5194/acp-2021-124.

Verreyken, B., Brioude, J., Evan, S., 2019. Development of turbulent scheme in the flexpart-arome v1.2.1 Lagrangian particle dispersion model. Geosci. Model Dev. (GMD) 12, 4245–4259. https://doi.org/10.5194/gmd-12-4245-2019.